

TECHNICAL UNIVERSITY OF CRETE  
ELECTRICAL AND COMPUTER ENGINEERING DEPARTMENT  
TELECOMMUNICATIONS DIVISION



# Localization in Environmental Scatter Radio Networks

by

Marios Vestakis

A THESIS SUBMITTED IN PARTIAL FULFILLMENT OF  
THE REQUIREMENTS FOR THE DIPLOMA OF  
ELECTRICAL AND COMPUTER ENGINEERING

July 2017

THESIS COMMITTEE

Associate Professor Aggelos Bletsas, *Thesis Supervisor*  
Associate Professor George N. Karystinos  
Associate Professor Antonios Deligiannakis

# Abstract

Scatter radio networks have been recently proposed for environmental sensing applications, e.g., water savings in agriculture. Additionally, they are central in inventory management with radio frequency identification (RFID) tags, as well as other Internet of Things (IoT) applications. Recent signal processing developments in bistatic scatter radio networks have dramatically extended their coverage; thus, knowing the location of each tag becomes valuable information. Each scatter radio tag reflects the illuminating signal, transmitted from multiple low-cost emitters. The received signal strength (RSS) measurements at a single low-cost reader are used as input in custom particle filtering (PF) algorithms, in order to localize each scatter radio tag. Free-space, two-ray and an empirical wireless propagation large-scale path loss models are considered, alongside a small-scale fading model and different particle resampling techniques. Extensive simulations for a  $100m \times 100m$  grid offered root mean squared error (RMSE) as low as  $1.6m$ . Outdoor experimental results in a  $27m \times 32m$  grid offered  $0.9m$  RMSE.

Thesis Supervisor: Associate Professor Aggelos Bletsas

# Acknowledgements

I would like to thank all my friends, my advisor and my family. I say friends because everyone in this group apart from being a colleague of mine, is definitely considered a friend. The atmosphere in the lab is very friendly and everyone is willing to help one another. I start from Panos Alevizos who spent many hours answering my questions always in a good mood, Georgios Vougioukas who was a big help for more technical matters, and everyone else, especially when we spent hours in order to take experimental measurements out in the sun. I feel the need to say a big thank you to my advisor Prof. Aggelos Bletsas for guiding me this last year and for the fact that whenever I had questions he would happily sit down with me and pass me his knowledge. Lastly I want to thank my family for supporting me throughout all my studies and always being there for me.

*To my family, my advisor and all my friends...*

# Table of Contents

<b>Table of Contents</b> . . . . .	4
<b>List of Figures</b> . . . . .	6
<b>1 Introduction</b> . . . . .	8
1.1 Sensor Localization In Environmental Scatter Radio Networks	8
<b>2 Environmental Scatter Radio Networks: Architecture</b> . . .	10
2.1 Problem Formulation & Bistatic Scatter Radio Networks . . .	10
2.2 Scatter Radio Modules . . . . .	11
2.2.1 Scatter Radio Tag . . . . .	11
2.2.2 Carrier Emitter . . . . .	12
2.2.3 Reader-Spectrum Analyzer . . . . .	13
<b>3 RSSI models and PF algorithms</b> . . . . .	15
3.1 Received Signal Strength Indication (RSSI) models . . . . .	15
3.1.1 Point-to-Point Wireless Link . . . . .	15
3.1.2 Emitter-to-Tag-to-Reader Wireless Link . . . . .	16
3.2 PF algorithms . . . . .	20
3.2.1 Particle Filter for HMMs . . . . .	20
3.2.2 Baseline model . . . . .	22
3.2.3 PF models with resampling . . . . .	23
<b>4 Results</b> . . . . .	26
4.1 Simulation Results . . . . .	26
4.2 Outdoor Experimental Results . . . . .	31

---

<b>5</b>	<b>Conclusions And Future Work</b>	36
5.1	Conclusions	36
5.2	Future Work	36
<b>6</b>	<b>Appendix</b>	37
6.1	Proof for Product of Two Gamma Distributions	37
	<b>Bibliography</b>	40

# List of Figures

1.1	A typical bistatic setup where the low cost emitter illuminates the ultra-low cost scatter tag and the tag uses the carrier signal to modulate the information. The low cost SDR reader (it can be an RTL with cost less than 5\$) receives and demodulates the signal in order to extract the information. . . . .	9
2.1	Bistatic Scatter Radio Network as described above. Time Division Multiple Access (TDMA) is assumed: Only one emitter illuminates the tag at a time. . . . .	10
2.2	ADG1919 switch (top red rectangle) controlled by a Tektronix AFG3021B (bottom red rectangle). . . . .	11
2.3	ADG1919 switch. . . . .	12
2.4	Tektronix AFG3021B. . . . .	12
2.5	Si1064 Wireless MCU Development Kit. . . . .	12
2.6	Si1064 Wireless dk set upped for the experiment. . . . .	13
2.7	Agilent N9912A spectrum analyzer. . . . .	13
2.8	Agilent N9912A spectrum analyzer set upped for the experiment. . . . .	14
3.1	A typical point-to-point link. . . . .	15
3.2	A typical bistatic link. . . . .	18
3.3	Example of an HMM. . . . .	20
4.1	RMSE comparison for baseline model with free-space model, resampling second model with free-space model and resampling second model with Two-ray model. It is clear that the Two-ray model returned better results compared to free-space model. . . . .	27

---

4.2	RMSE comparison for free-space model with different resampling methods. The second resampling method is more efficient.	28
4.3	RMSE comparison for Two-ray model with different resampling methods. The second resampling method is again more efficient. . . . .	29
4.4	RMSE for free-space model with baseline method as the number of particles $M$ is increasing. The number of measurements per Epoch is fixed at 100 and grid size is $100m \times 100m$ . . . . .	30
4.5	First setup from satellite, located at the garden of the ECE department of Technical university of Crete. The red dots are the emitters, the blue dot is the reader and the black one is the tag to be localized. . . . .	31
4.6	Localization of scatter tag with 500 real measurements and number of particles $M = 1000$ , resulting in 0.9 meters error on $27m \times 32m$ grid which is quite impressive. Free-space model is assumed and the second resampling method is used. . . . .	32
4.7	Localization of scatter tag with 500 real measurements and number of particles $M = 1000$ , resulting in 1.42 meters error on $27m \times 32m$ grid. Free-space model is assumed and the baseline method is used. . . . .	33
4.8	Second setup from satellite. The red dots are the emitters, the blue dot is the reader and the black one is the tag to be localized. . . . .	33
4.9	Localization of scatter tag with real measurements and number of particles $M = 1000$ , resulting in 5.6 meters error on $17m \times 22m$ grid. Free-space model is assumed and the second resampling method (with $\sigma=1.3m$ for the Gaussian) is used.	34
4.10	Localization of scatter tag with real measurements and number of particles $M = 1000$ , resulting in 5.61 meters error on $17m \times 22m$ grid. Free-space model is assumed and the baseline method is used. . . . .	35

# Chapter 1

## Introduction

### 1.1 Sensor Localization In Environmental Scatter Radio Networks

Conventional Marconi radios use active, power hungry components like amplifiers, mixers and oscillators, in contrast, scatter radio tags use just ultra-low power transistor(s) (RF switch(es)) that alter(s) the termination of the antenna, thus requiring minimum power consumption to achieve communication [1]. A tag is illuminated by a carrier and the alternation of the loads terminating the tag's antenna causes reflection of the impinged carrier. Depending on the selected load and the alternation methods, different modulation schemes can be achieved.

Scatter Radio Networks are developed due to their ultra low power consumption (they can be battery-less with a small solar panel [2], or even with RF harvesting [3]) and their ultra-low cost [4]. Large-scale wireless sensor networks are primarily employed for low-cost, ubiquitous sensing of environmental variables, such as, temperature, soil moisture, and luminosity. In the context of agricultural monitoring they can offer large benefits to the farmer, including precision agriculture with low monetary cost. In depth monitoring of the field leads to decreased water consumption, which has both economic and environmental benefit [5, 6].

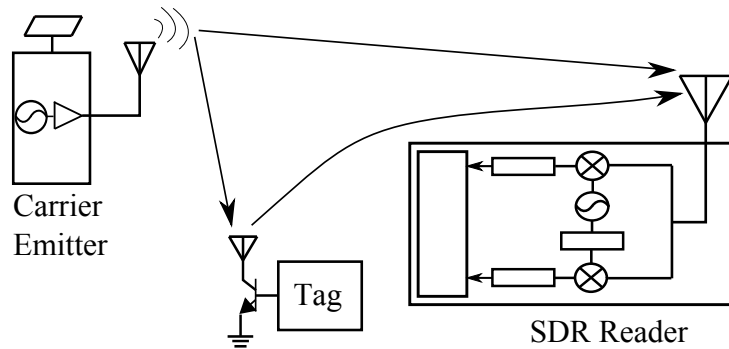


Figure 1.1: A typical bistatic setup where the low cost emitter illuminates the ultra-low cost scatter tag and the tag uses the carrier signal to modulate the information. The low cost SDR reader (it can be an RTL with cost less than 5\$) receives and demodulates the signal in order to extract the information.

The goal of this thesis is to estimate the location of a tag that is potentially placed anywhere across a field, which apart from the scientific interest, it also has practical value because of the scatter radio sensor’s ultra-low cost. For instance, there could be hundreds of sensors plugged in the soil or on the plants which is increasing the need for localizing them. The question is why not use a Global Positioning System (GPS) on each tag and the answer is that GPS and ultra-low cost do not come in the same sentence in this application, (e.g., GPS cost approximately 10\$), since the goal of the scatter radio sensor network is to be as large as possible.

Apart from that, RF localization could find application in areas where GPS signal is weak, e.g., big cities with tall buildings have many blind spots that deteriorate the performance of GPS.

On the other hand, RSS-based localization is a very challenging problem to be solved, especially on scatter radio networks since the communication model changes from classic Marconi-radio point-to-point system to a more complex bistatic scatter radio model.

In the following chapter an overall image of the problem will be given, presenting both the problem formulation and the testbed that was used. Moreover this work emphasizes on localization through custom PF algorithms based on RSS measurements. Finally, both simulation and experimental results are presented to validate the efficiency of the proposed algorithms.

# Chapter 2

## Environmental Scatter Radio Networks: Architecture

### 2.1 Problem Formulation & Bistatic Scatter Radio Networks

The scatter radio network consists of  $N$  carrier emitters, one RF tag to be localized and one reader (spectrum analyzer). In contrast to Marconi radios that are used in everyday life (cellphones), scatter radios modulate information on the incoming carrier signal from the emitter. Thus the power consumption of the scatter tag is dramatically reduced since the modulation is achieved through a switch. The Reader logs the received power in a specified band of bandwidth  $W_R$  around a specified center frequency  $F_R = F_c + F_{sw}$ , where  $F_C = 868\text{MHz}$  and  $F_{sw} \sim 250\text{KHz}$ .

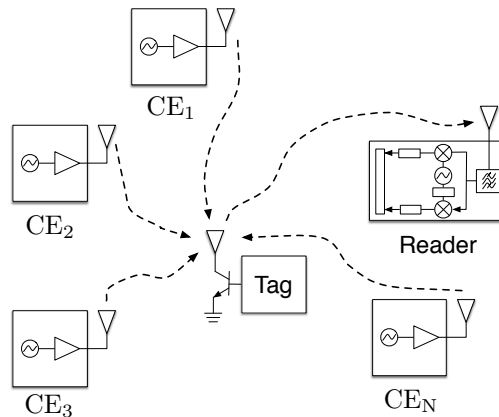


Figure 2.1: Bistatic Scatter Radio Network as described above. Time Division Multiple Access (TDMA) is assumed: Only one emitter illuminates the tag at a time.

More specifically the location of each emitter  $j$  is defined,  $\mathbf{x}_j \triangleq [x_j \ y_j]^T$ ,  $\forall j = 1 \dots N$  and the location of the reader is defined,  $\mathbf{x}_R \triangleq [x_R \ y_R]^T$  are both known and fixed. The immobile location of the tag that is to be estimated is defined,  $\mathbf{x}_T \triangleq [x_T \ y_T]^T$  [7].

## 2.2 Scatter Radio Modules

In order to take measurements for this work, the experimental setup was deployed consisting of a scatter radio tag, an emitter and a reader.

### 2.2.1 Scatter Radio Tag

The tag used in this experiment is actually an ADG1919 switch controlled by a Tektronix AFG3021B, configured to produce square waves with  $f_{sw} = 250\text{KHz}$  at levels 0 to 2.2V.



Figure 2.2: ADG1919 switch (top red rectangle) controlled by a Tektronix AFG3021B (bottom red rectangle).



Figure 2.3: ADG1919 switch.



Figure 2.4: Tektronix AFG3021B.

### 2.2.2 Carrier Emitter

The carrier emitter is a Si1064 Wireless MCU Development Kit, operating in the European UHF ISM band (865-868 MHz) tuned to emit at power +12.1dBm (without the antenna gain).

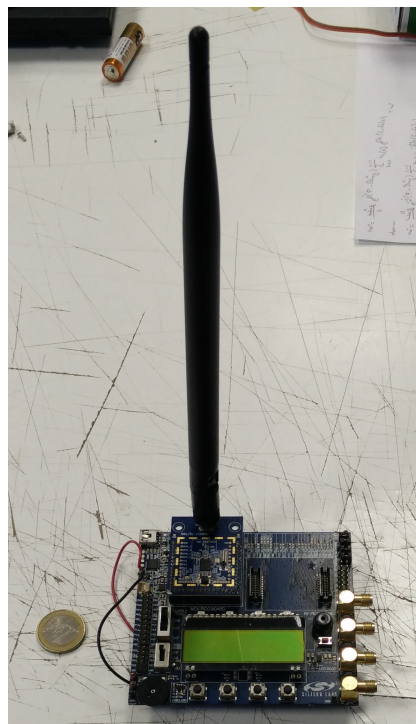


Figure 2.5: Si1064 Wireless MCU Development Kit.



Figure 2.6: Si1064 Wireless dk set upped for the experiment.

### 2.2.3 Reader-Spectrum Analyzer

The reader in this setup is an Agilent N9912A spectrum analyzer configured to lay channel power.



Figure 2.7: Agilent N9912A spectrum analyzer.



Figure 2.8: Agilent N9912A spectrum analyzer set upped for the experiment.

# Chapter 3

## RSSI models and PF algorithms

### 3.1 Received Signal Strength Indication (RSSI) models

The spectrum analyzer records  $N \times T$  i.i.d. RSS measurements  $y_j^{[t]}$ ,  $j = 1 \dots N$  and  $t = 1 \dots T$ , where  $N$  is the number of emitters and  $T$  the number of measurements for each emitter-to-tag-to-reader link. Two models for the wireless links are assumed: free-space propagation and Two-ray model.

#### 3.1.1 Point-to-Point Wireless Link

Below is depicted a typical **point-to-point link**, where the transmitter sends a signal with transmission power  $P_{TX}$  ( $\simeq 12\text{dBm}$ ) with isotropic antenna gain  $G_{TX}$  (2.15 dBi). According to the **free-space model** the received power at the end of the reader is given by the equation:

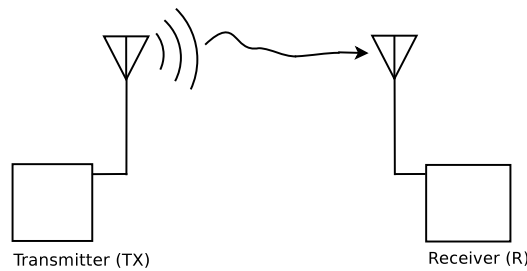


Figure 3.1: A typical point-to-point link.

$$P_R = P_{TX} G_{TX} G_R \left( \frac{\lambda}{4\pi \|\mathbf{x}_R - \mathbf{x}_{TX}\|_2} \right)^2, \quad (3.1)$$

where  $G_R$  is the receiver antenna gain (2.15 dBi),  $\lambda = \frac{c}{f_c}$  is the wave length and  $\|\mathbf{x}_R - \mathbf{x}_{TX}\|_2$  is the distance between the transmitter and the reader.

The second approach is based on the **Two-ray model**, where the equations change according to threshold  $d_0 = \frac{4\pi h_T h_R}{\lambda}$ ; thus, for  $\|\mathbf{x}_R - \mathbf{x}_{TX}\|_2 < d_0$  the equation for  $P_R$  is the same as the free-space model shown above, while for  $\|\mathbf{x}_R - \mathbf{x}_{TX}\|_2 \geq d_0$ :

$$P_R = P_{TX} G_{TX} G_R \left( \frac{h_R h_{TX}}{\|\mathbf{x}_R - \mathbf{x}_{TX}\|_2^2} \right)^2, \quad (3.2)$$

where  $h_R, h_{TX}$  are the height of the antenna of the reader and of the transmitter, respectively.

### 3.1.2 Emitter-to-Tag-to-Reader Wireless Link

In this case study Nakagami small-scale fading is assumed. The amplitude of fading coefficients from emitter to tag and tag-to-reader, denoted as  $|h_j|$  and  $|h_{0,j}|$ , respectively and are assumed Nakagami random variables; thus,  $|H_j|^2 = |h_j|^2 |h_{0,j}|^2$  is the product of two Gamma random variables.

**Theorem:**

$$\begin{aligned} |h_j|^2 &\equiv \gamma_1 \sim \Gamma\left(m_{1,j}, \frac{1}{m_{1,j}}\right), \\ |h_{0,j}|^2 &\equiv \gamma_2 \sim \Gamma\left(m_2, \frac{1}{m_2}\right) \end{aligned}$$

$$x = \gamma_1 \gamma_2, \text{ with } \gamma_1 \perp \gamma_2,$$

where  $\Gamma(k, \theta)$  is the gamma distribution with shape parameter  $k$  and scale parameter  $\theta$ . In addition  $\gamma_1$  and  $\gamma_2$  are independent and of unit-mean Gamma random variables.

$$\begin{aligned} f_x(x) &= \\ &= \frac{m_{1,j}^{m_{1,j}} m_2^{m_2} x^{m_2-1}}{\Gamma(m_{1,j}) \Gamma(m_2)} 2 \left( \frac{m_2 x}{m_{1,j}} \right)^{\frac{m_{1,j}-m_2}{2}} K_{m_{1,j}-m_2} \left( 2\sqrt{m_{1,j} m_2 x} \right), \end{aligned} \quad (3.3)$$

where  $K_\nu(\cdot)$  is the modified Bessel function of the second kind.

**Corollary:**

$$y = a_j^{[m]} x = a_j^{[m]} \gamma_1 \gamma_2$$

and

$$a_j^{[m]} = P_{TX} L_j(\mathbf{x}_T^{[m]}) L_0(\mathbf{x}_T^{[m]}) \quad (3.4)$$

$$\begin{aligned} f_{y|\mathbf{x}_t^{[m]}}(y; a_j^{[m]}, m_{1,j}, m_2) &= \\ &= 2 \left( \frac{m_{1,j} m_2}{a_j^{[m]}} \right)^{\frac{m_{1,j}+m_2}{2}} y^{\frac{m_{1,j}+m_2}{2}-1} \frac{1}{\Gamma(m_{1,j}) \Gamma(m_2)} K_{m_{1,j}-m_2} \left( 2\sqrt{\frac{m_{1,j} m_2 y}{a_j^{[m]}}} \right) \end{aligned} \quad (3.5)$$

See Appendix for the proof.

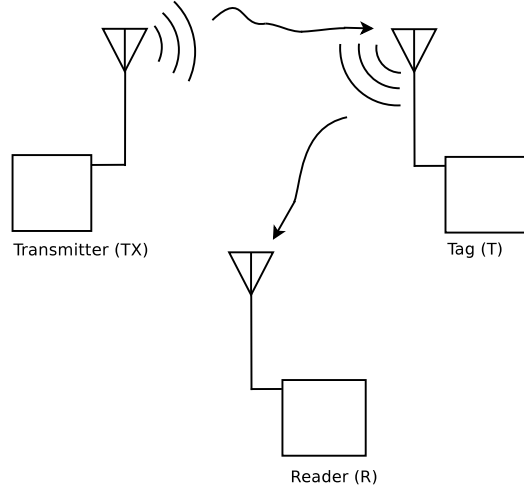


Figure 3.2: A typical bistatic link.

According to the **free-space model** the path loss for the two links are:

$$L_j(\mathbf{x}_T) = G_{TX_j} G_T \left( \frac{\lambda}{4\pi \|\mathbf{x}_T - \mathbf{x}_j\|_2} \right)^2 \quad (3.6)$$

$$L_0(\mathbf{x}_T) = G_T G_R \left( \frac{\lambda}{4\pi \|\mathbf{x}_R - \mathbf{x}_T\|_2} \right)^2, \quad (3.7)$$

where  $L_j$  and  $L_0$  are the path loss of the emitter-to-tag link and of the tag-to-reader link, respectively.

$$y_j^{[t]} \equiv y_j^{[t]}(\mathbf{x}_T) = P_{TX} L_j(\mathbf{x}_T) L_0(\mathbf{x}_T) \eta_T |h_j^{[t]}|^2 |h_{0,j}^{[t]}|^2, \quad (3.8)$$

where  $\eta_T$  is the scattering efficiency constant of the tag with value 0.1.

According to the **Two-ray model** the path loss equations change to:

For  $\|\mathbf{x}_T - \mathbf{x}_j\|_2 < d_0$ :

$$L_j(\mathbf{x}_T) = G_{TX} G_T \left( \frac{\lambda}{4\pi \|\mathbf{x}_T - \mathbf{x}_j\|_2} \right)^2 \quad (3.9)$$

For  $\|\mathbf{x}_T - \mathbf{x}_j\|_2 \geq d_0$

$$L_j(\mathbf{x}_T) = G_{TX}G_T \left( \frac{h_T h_R}{\|\mathbf{x}_T - \mathbf{x}_j\|_2^2} \right)^2 \quad (3.10)$$

For  $\|\mathbf{x}_R - \mathbf{x}_T\|_2 < d_0$ :

$$L_0(\mathbf{x}_T) = G_T G_R \left( \frac{\lambda}{4\pi\|\mathbf{x}_R - \mathbf{x}_T\|_2} \right)^2 \quad (3.11)$$

For  $\|\mathbf{x}_R - \mathbf{x}_T\|_2 \geq d_0$ :

$$L_0(\mathbf{x}_T) = G_T G_R \left( \frac{h_T h_R}{\|\mathbf{x}_R - \mathbf{x}_T\|_2^2} \right)^2 \quad (3.12)$$

While the received power equation remains the same as 3.8.

**Empirical Path Loss Model.** In this model the pathloss exponents  $\nu_j$  &  $\nu_0$  are estimated. This estimation is achieved through particle filtering and the equations are:

$$L_j(\mathbf{x}_T) = G_{TX}G_T K \left( \frac{1}{\|\mathbf{x}_T - \mathbf{x}_j\|_2} \right)^{\nu_j} \quad (3.13)$$

$$L_0(\mathbf{x}_T) = G_T G_R K \left( \frac{1}{\|\mathbf{x}_R - \mathbf{x}_T\|_2} \right)^{\nu_0}, \quad (3.14)$$

where  $K = \left(\frac{\lambda}{4\pi}\right)^2$

$$y_j^{[t]} = P_{TX} L_j(\mathbf{x}_T) L_0(\mathbf{x}_T) \eta_T |h_j^{[t]}|^2 |h_{0,j}^{[t]}|^2 \quad (3.15)$$

## 3.2 PF algorithms

In this work two different PF algorithms were implemented, one with no resampling and one with. For the latter, three different versions were put to test and will be thoroughly presented in this section.

### 3.2.1 Particle Filter for HMMs

Consider an HMM with general continuous state and observation distributions as depicted below: we want to estimate hidden states  $x_0, \dots, x_T$  given associated observations  $y_0, \dots, y_T$  (measurements).

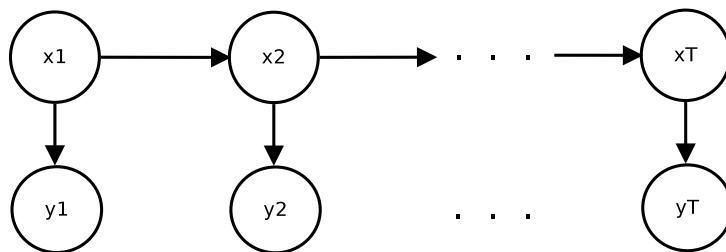


Figure 3.3: Example of an HMM.

However, samples cannot be drawn directly from  $p_{x_t|y_0 \dots y_T}(x_t|y_0 \dots y_T)$ ,  $0 \leq t \leq T$ . We are given a distribution with density  $\mu$  such that

$$\mu(x) = \frac{q(x)}{Z}, \quad (3.16)$$

where  $q(x)$  is a known function and  $Z$  is unknown normalization constant. It is needed to sample from  $\mu$  in order to estimate

$$\mathbb{E}[f(x)] = \int f(x) \mu(x) dx. \quad (3.17)$$

Samples (particles) can be drawn from a known distribution with density  $\nu$ , potentially very different from  $\mu$ . Importance sampling provides means to solve this problem:

- Sample  $x(1), \dots, x(M)$  from a known distribution with density  $\nu$ .

- Compute  $w(1), \dots, w(M)$  as

$$w(m) = \frac{q(x(m))}{\nu(x(m))} = \prod_{t=1}^T p_{y_t|x_t}(y_t|x_t) \quad (3.18)$$

- output estimation for  $\mathbb{E}_\mu[f(x)]$  as

$$\hat{\mathbb{E}}(M) = \frac{\sum_{m=1}^M w(m) f(x(m))}{\sum_{m=1}^M w(m)} \quad (3.19)$$

As  $M \rightarrow \infty$ , the estimation  $\hat{\mathbb{E}}(M)$  converges to the desired value  $\mathbb{E}_\mu[f(x)]$ . Let support of distribution with density  $p$  be

$$\text{supp}(p) = \{x : p(x) > 0\}. \quad (3.20)$$

**Theorem.** Let  $\text{supp}(\mu) \subseteq \text{supp}(\nu)$ . Then as  $M \rightarrow \infty$ ,

$$\hat{\mathbb{E}}(M) \rightarrow \mathbb{E}_\mu[f(x)], \text{ with probability 1,} \quad (3.21)$$

**Proof.** Using strong law of large numbers, it follows that with probability 1,

$$\begin{aligned} \frac{1}{M} \sum_{m=1}^M w(m) f(x(m)) &\rightarrow \mathbb{E}_\nu \left[ \frac{q(x)}{\nu(x)} f(x) \right] \\ &= \int_{\text{supp}(\nu)} \frac{q(x)}{\nu(x)} f(x) \nu(x) dx \\ &= \int_{\text{supp}(\mu)} Z \mu(x) f(x) dx \\ &= Z \mathbb{E}_\mu[f(x)], \end{aligned} \quad (3.22)$$

where it has been used the fact that  $q(x) = 0$  for  $x \notin \text{supp}(\mu)$ . Using similar argument it follows that with probability 1,

$$\frac{1}{M} \sum_{m=1}^M w(m) \rightarrow Z \mathbb{E}_\mu[1] = Z. \quad (3.23)$$

Leading to the desired conclusion.

**Remarks.** It is worth noting that as long as  $\text{supp}(\mu)$  is contained in  $\text{supp}(\nu)$ , the estimation converges irrespective of choice of  $\nu$ . This is quite remarkable. Alas, it comes at a cost. The choice of  $\nu$  determines the variance of the estimator and hence the number of samples  $M$  required to obtain good estimation.

### 3.2.2 Baseline model

$$p(\mathbf{y}|\boldsymbol{\chi}_t^{[m]}) = \prod_{t=1}^T \prod_{j=1}^N f_{y_j^{[t]}|\boldsymbol{\chi}_t^{[m]}}(y_j^{[t]}|\boldsymbol{\chi}_t^{[m]}), \quad (3.24)$$

where  $\boldsymbol{\chi}_t^{[m]} = [x_T^{[m]} \ y_T^{[m]}]$ ,  $^{[m]}$  is the particle index and  $\mathbf{y}$  contains  $N \times T$  RSS measurements.

- 1: **Initialization of Variables:**
- 2: Set  $M$  (number of Particles)
- 3:  $X_a, Y_a$  (dimensions of the area),  $T$  (time window)
- 4: **for**  $epoch = 1 : E$  **do**
- 5:     **Initialization of Particles:**,  $\forall m = 1 : M$
- 6:          $x_{t=0}^{[m]} \sim \mathcal{U}[0, X_a]$ ,  $y_{t=0}^{[m]} \sim \mathcal{U}[0, Y_a]$
- 7:          $\boldsymbol{\chi}_{t=0}^{[m]} = [x_T^{[m]} \ y_T^{[m]}]^T$
- 8:         **Select**  $T$  measurements  $\{y_j^{[t]}\} \forall$  emitter  $j$
- 9:         **for**  $m = 1 : M$  **do** { particle index }
- 10:              $w^{[m]} = p(\mathbf{y}|\boldsymbol{\chi}_t^{[m]})$
- 11:         **end for**
- 12:         Normalize weights  $w^{[m]}$ ,  $m = 1 \dots M$
- 13:         **Result** $_{\boldsymbol{\chi}_{1:T}|\mathbf{y}}^{[epoch]} = \sum_{m=1}^M w_{1:T}^{[m]} \boldsymbol{\chi}_{1:T}^{[m]}$
- 14:     **end for**
- 15: **Estimate**  $= \mathbb{E} \left[ \mathbf{Result}_{\boldsymbol{\chi}_{1:T}|\mathbf{y}}^{[1:E]} \right]$

Each epoch is an independent experiment, with different and independent set of measurements.

### 3.2.3 PF models with resampling

$$p\left(\mathbf{y}^{[t]}|\boldsymbol{\chi}_t^{[m]}\right) = \prod_{j=1}^N f_{y_j^{[t]}|\boldsymbol{\chi}_t^{[m]}}\left(y_j^{[t]}|\boldsymbol{\chi}_t^{[m]}\right) \quad (3.25)$$

**First resampling method:** [8]

- 1: **Initialization of Variables:**
- 2: Set  $M$  (number of Particles)
- 3:  $X_a, Y_a$  (dimensions of the area),  $T$  (time window)
- 4: **for**  $epoch = 1 : E$  **do**
- 5:     **Initialization of Particles;**,  $\forall m = 1 : M$
- 6:          $x_{t=0}^{[m]} \sim \mathcal{U}[0, X_a]$ ,  $y_{t=0}^{[m]} \sim \mathcal{U}[0, Y_a]$
- 7:          $\boldsymbol{\chi}_{t=0}^{[m]} = \begin{bmatrix} x_T^{[m]} & y_T^{[m]} \end{bmatrix}^T$
- 8:     **Select**  $T$  measurements  $\{y_j^{[t]}\} \forall$  emitter  $j$
- 9:     **for**  $t = 1 : T$  **do** {time-step}
- 10:         **for**  $m = 1 : M$  **do** { particle index }
- 11:             **if**  $t > 1$
- 12:                 Sample  $\boldsymbol{\chi}_t^{[m]} \sim \mathcal{N}\left(\mathbb{E}\left[\boldsymbol{\chi}_{t-1}^{[1:M_1]}\right], \sigma^2 \mathbf{I}_2\right)$
- 13:             **end if**
- 14:              $w_t^{[m]} = p\left(\mathbf{y}_j^{[t]}|\boldsymbol{\chi}_t^{[m]}\right)$
- 15:             **end for**
- 16:         Normalize weights  $\mathbf{w}_t^{[1:M]}$
- 17:          $\boldsymbol{\chi}_t^{[1:M_1]} \leftarrow$  Low-Variance Sampler $\left(\boldsymbol{\chi}_t^{[1:M]}, \mathbf{w}_t^{[1:M]}\right)$  [9]
- 18:     **end for**
- 19:     Re-normalize Weights  $\mathbf{w}_T^{[1:M_1]}$
- 20:     **Result** $_{\boldsymbol{\chi}_T|y_T}^{[epoch]} = \sum_{m=1}^{M_1} w_T^{[m]} \boldsymbol{\chi}_T^{[m]}$
- 21: **end for**
- 22: **Estimate**  $= \mathbb{E}\left[\mathbf{Result}_{\boldsymbol{\chi}_T|y_T}^{[1:E]}\right]$

From [line 12](#):  $\sigma^2 = 3.3^2$ .

Generating all particles with a Gaussian with mean the expected value of the particles that "survived" the resampling process and with variance experimentally chosen, is a heuristic method which works excellent for small

number of particles  $M$  4.1.

From line 17:

```

1: Algorithm Low-variance sampler ( $\chi_t, \mathbf{w}_t$ ):
2:  $\bar{\chi}_t = 0$ 
3:  $c = w_t^{[1]}$ 
4:  $i = 1$ 
5: for  $m = 1 : M$  do
6:    $u = r + (m - 1) M^{-1}$ 
7:   while  $u > c$ 
8:      $i = i + 1$ 
9:      $c = c + w_t^{[i]}$ 
10:  end while
11:  add  $x_t^{[i]}$  to  $\bar{\chi}_t$ 
12: end for
13: return  $\bar{\chi}_t$ 

```

### Second resampling method:

```

1: Initialization of Variables:
2: Set  $M$  (number of Particles)
3:  $X_a, Y_a$  (dimensions of the area),  $T$  (time window)
4: for  $epoch = 1 : E$  do
5:   Initialization of Particles:,  $\forall m = 1 : M$ 
6:      $x_{t=0}^{[m]} \sim \mathcal{U}[0, X_a], y_{t=0}^{[m]} \sim \mathcal{U}[0, Y_a]$ 
7:      $\chi_{t=0}^{[m]} = [x_T^{[m]} \ y_T^{[m]}]^T$ 
8:     Select  $T$  measurements  $\{y_j^{[t]}\} \forall$  emitter  $j$ 
9:     for  $t = 1 : T$  do {time-step}
10:      for  $m = 1 : M$  do { particle index }
11:        if  $t > 1$ 
12:           $\chi_t^{[1:M_1]} = \chi_{t-1}^{[1:M_1]}$ 
13:          if  $m > M_1$ 
14:            Sample  $\chi_t^{[m]} \sim \mathcal{N} \left( \mathbb{E} \left[ \chi_{t-1}^{[1:M_1]} \right], \sigma^2 \mathbf{I}_2 \right)$ 
15:          end if

```

---

```

16:         end if
17:          $w_t^{[m]} = p(\mathbf{y}_j^{[t]} | \boldsymbol{\chi}_t^{[m]})$ 
18:     end for
19:     Normalize weights  $\mathbf{w}_t^{[1:M]}$ 
20:      $\boldsymbol{\chi}_t^{[1:M_1]} \leftarrow \text{Low-Variance Sampler}(\boldsymbol{\chi}_t^{[1:M]}, \mathbf{w}_t^{[1:M]})$  [9]
21: end for
22: Re-normalize Weights  $\mathbf{w}_T^{[1:M_1]}$ 
23: Result $_{\boldsymbol{\chi}_T|y_T}^{[epoch]} = \sum_{m=1}^{M_1} w_T^{[m]} \boldsymbol{\chi}_T^{[m]}$ 
24: end for
25: Estimate =  $\mathbb{E} \left[ \mathbf{Result}_{\boldsymbol{\chi}_T|y_T}^{[1:E]} \right]$ 
    From line 14:  $\sigma^2 = 3.3^2$ .

```

The difference from the previous version of the algorithm is that the  $M_1$  particles that "survive" the resampling process are stored in  $\boldsymbol{\chi}_t^{[1:M_1]}$  and the rest  $M - M_1$  particles are generated with the same process as before with the Gaussian.

**Third resampling method:**

In this version of the algorithm the  $M - M_1$  particles are generated uniformly anywhere across the grid, in the exact way as the initialization. Apart from that version two and three are completely the same.

# Chapter 4

## Results

### 4.1 Simulation Results

This chapter presents the evaluation of the different PF models as well as the different RSS models, which were thoroughly described in the previous chapter.

In the figure depicted below, the number of particles  $M = 100$ , the number of independent experiments Epoch= 4000 and grid size is  $100m \times 100m$ . In order to evaluate each model, the tag's real location was randomly initialized anywhere across the grid for every Epoch.

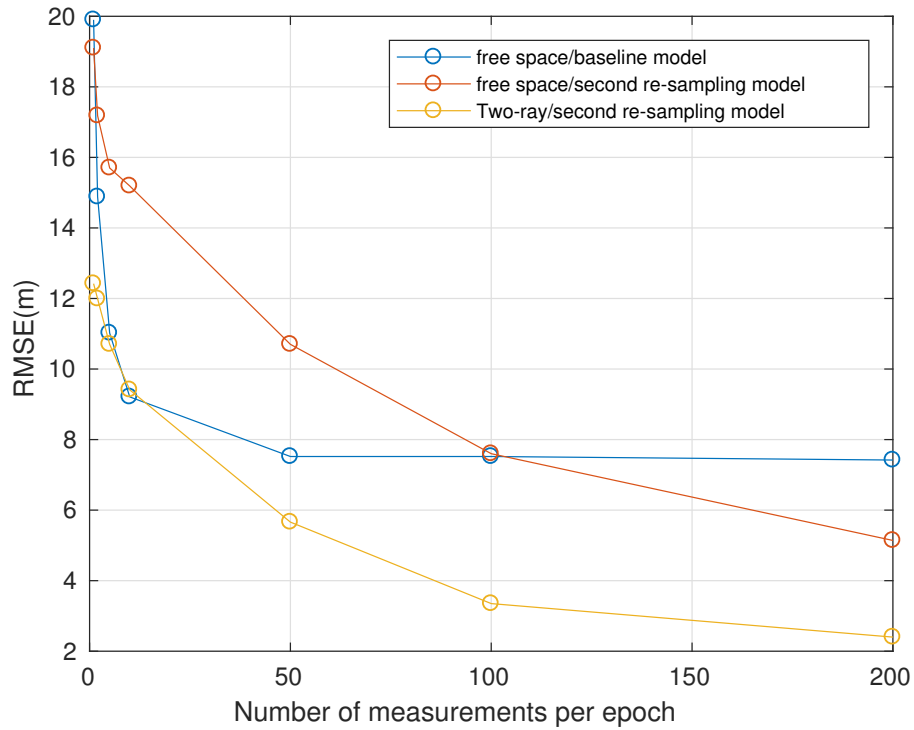


Figure 4.1: RMSE comparison for baseline model with free-space model, resampling second model with free-space model and resampling second model with Two-ray model. It is clear that the Two-ray model returned better results compared to free-space model.

In the next figure there is a comparison between the different resampling methods for the free-space model.

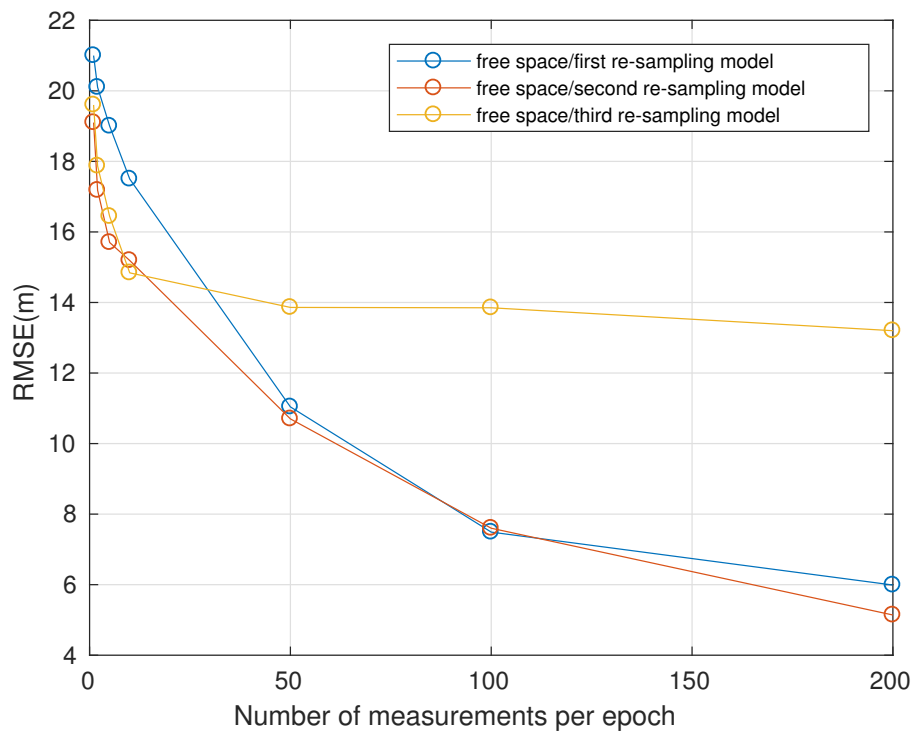


Figure 4.2: RMSE comparison for free-space model with different resampling methods. The second resampling method is more efficient.

In the next figure there is a comparison between the different resampling methods for the Two-ray model.

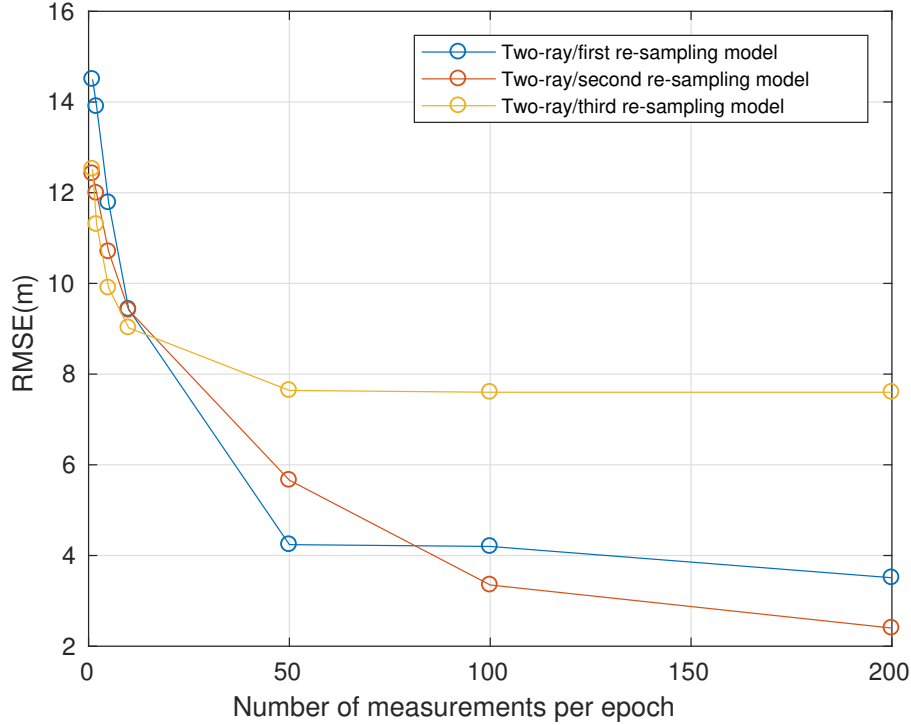


Figure 4.3: RMSE comparison for Two-ray model with different resampling methods. The second resampling method is again more efficient.

Apart from increasing the number of measurements while keeping the number of particles  $M$  fixed, more simulations were made to see the effect of a larger number of particles to the models. The results showed that the baseline model worked better every time  $M$  increased. On the other hand the PF algorithms with resampling, due to the heuristics (Gaussian), did not reduce the RMSE as  $M$  was increasing. That happened because the variance of the Gaussian that was used to generate the new particles was experimentally selected for fixed  $M$ ; so, as  $M$  increased, variance had to increase too in order to reduce the RMSE.

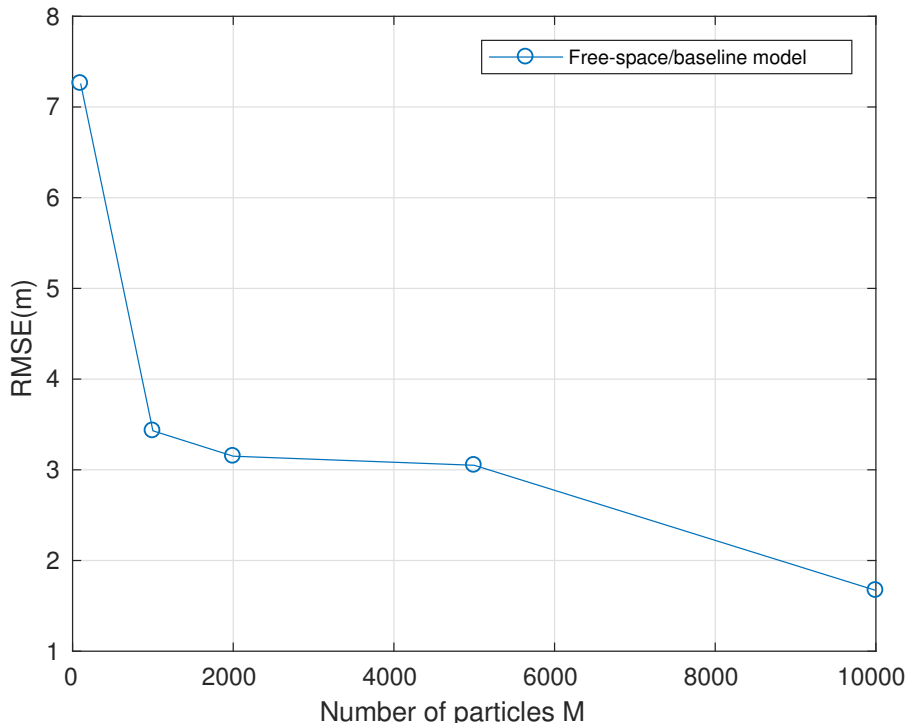


Figure 4.4: RMSE for free-space model with baseline method as the number of particles  $M$  is increasing. The number of measurements per Epoch is fixed at 100 and grid size is  $100m \times 100m$ .

**The empirical path loss model** is not compared to the other models, due to the bad simulation results. So just to be referenced it had, 20m RMSE which is nowhere near to the other models. The algorithm implemented for this model was 25 with a few additions:

below line 6:

I)  $\nu_{j,t=0}^{[m]} \sim \mathcal{U}[2, 2 + \delta]$

II)  $\nu_{0,t=0}^{[m]} \sim \mathcal{U}[2, 2 + \delta]$ , where  $\delta = 0.5$

and line 7 changes to:  $\boldsymbol{\chi}_{t=0}^{[m]} = [x_{\text{T}}^{[m]} \ y_{\text{T}}^{[m]} \ \nu_1^{[m]} \ \dots \ \nu_N^{[m]} \ \nu_0^{[m]}]^T$ .

In order to work properly, very good initialization of the  $\nu_1^{[m]} \dots \nu_N^{[m]} \ \nu_0^{[m]}$  was needed, because even a small error in the exponent estimation was fatal for the localization, which is normal since it is an exponent.

## 4.2 Outdoor Experimental Results

All the models did quite well in simulations, but they had to be put to test in an experimental setup. Two different setups were utilized, the first with reader location  $\mathbf{x}_R = [0 \ 9.6]^T$ , tag real location  $\mathbf{x}_T = [2.9 \ 9.6]^T$  and

emitters location  $\begin{bmatrix} \mathbf{x}_1^T \\ \mathbf{x}_2^T \\ \mathbf{x}_3^T \end{bmatrix} = \begin{bmatrix} 0 & 31.6 \\ 26.3 & 9.6 \\ 2.9 & 0 \end{bmatrix}$ . Five hundred measurements for

each emitter-to-tag-to-reader link were gathered and were used as input in the algorithms shown in the previous chapters.

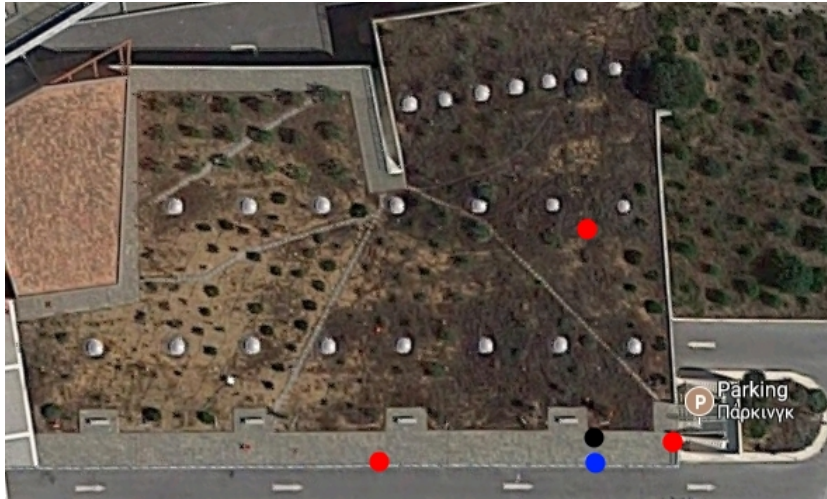


Figure 4.5: First setup from satellite, located at the garden of the ECE department of Technical university of Crete. The red dots are the emitters, the blue dot is the reader and the black one is the tag to be localized.

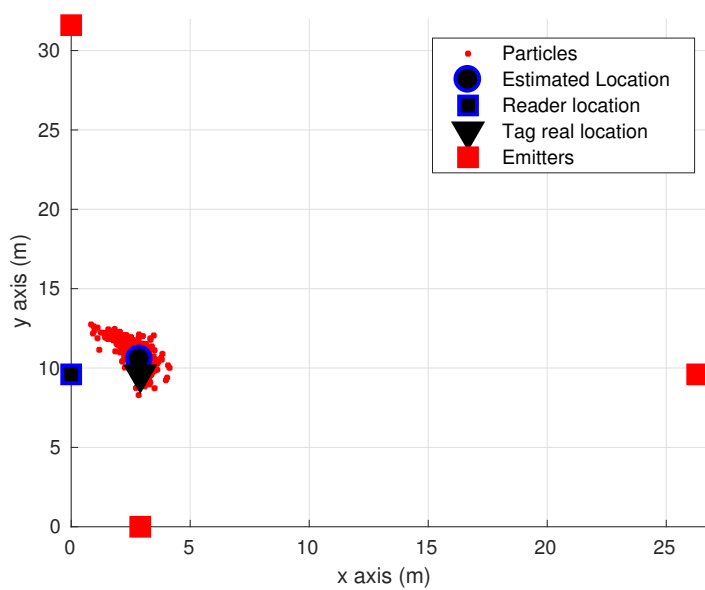


Figure 4.6: Localization of scatter tag with 500 real measurements and number of particles  $M = 1000$ , resulting in 0.9 meters error on  $27m \times 32m$  grid which is quite impressive. Free-space model is assumed and the second resampling method is used.

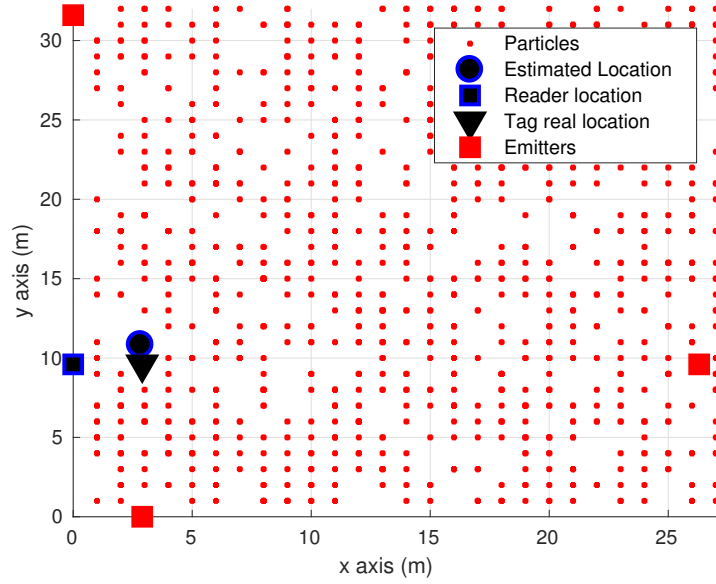


Figure 4.7: Localization of scatter tag with 500 real measurements and number of particles  $M = 1000$ , resulting in 1.42 meters error on  $27m \times 32m$  grid. Free-space model is assumed and the baseline method is used.

**Second setup:** with reader location  $\mathbf{x}_R = [0 \ 0]^T$ , tag real location

$$\mathbf{x}_T = [2.9 \ 13.5]^T \text{ and emitters location } \begin{bmatrix} \mathbf{x}_1^T \\ \mathbf{x}_2^T \\ \mathbf{x}_3^T \end{bmatrix} = \begin{bmatrix} 0 & 20.8 \\ 15.8 & 13.5 \\ 5.6 & 3.4 \end{bmatrix}.$$

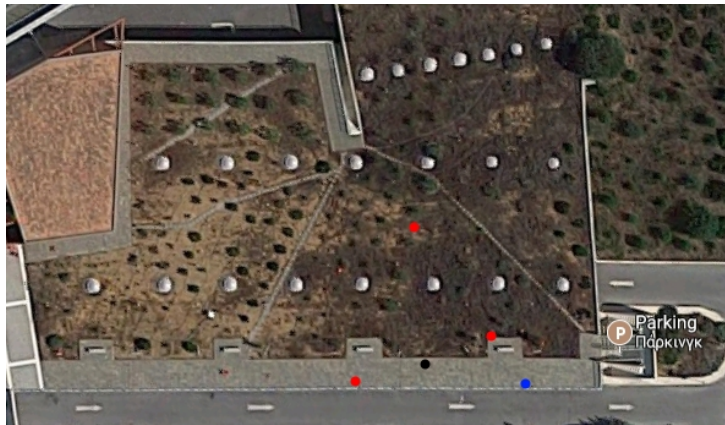


Figure 4.8: Second setup from satellite. The red dots are the emitters, the blue dot is the reader and the black one is the tag to be localized.

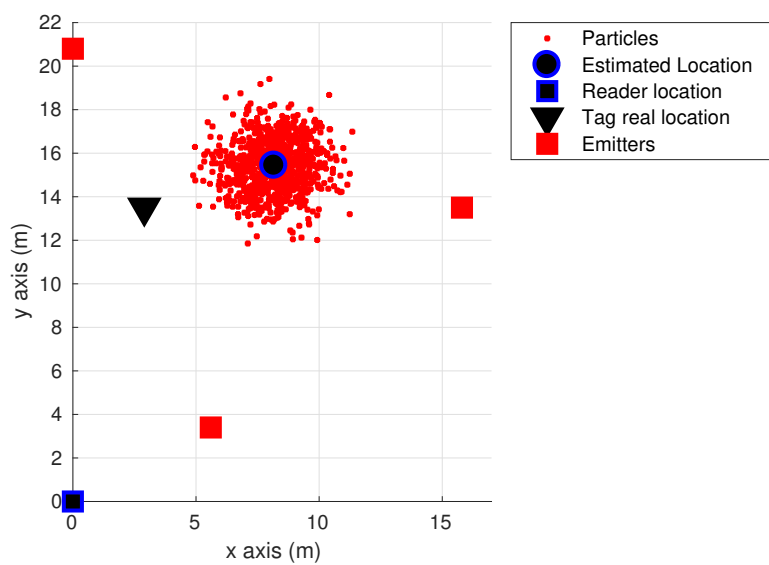


Figure 4.9: Localization of scatter tag with real measurements and number of particles  $M = 1000$ , resulting in 5.6 meters error on  $17m \times 22m$  grid. Free-space model is assumed and the second resampling method (with  $\sigma=1.3m$  for the Gaussian) is used.

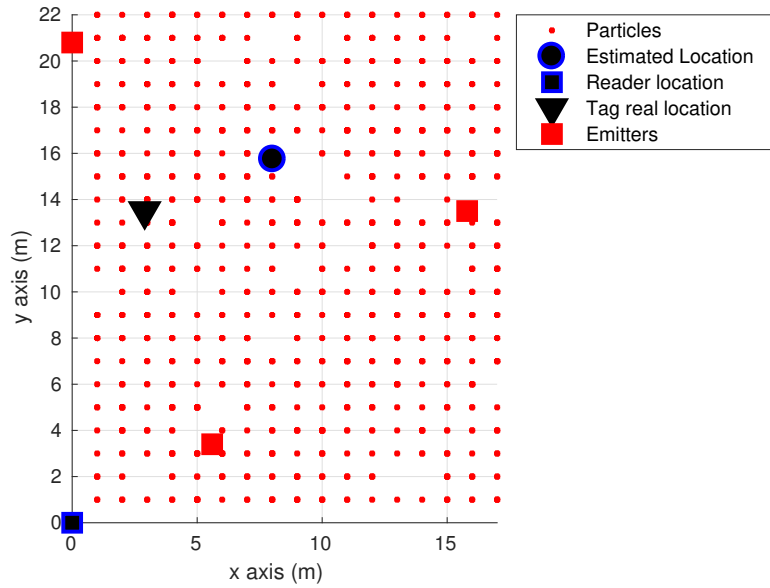


Figure 4.10: Localization of scatter tag with real measurements and number of particles  $M = 1000$ , resulting in 5.61 meters error on  $17m \times 22m$  grid. Free-space model is assumed and the baseline method is used.

The second setup had worse results due to the bigger distance between the tag and the reader ( $13.8m$ ), in comparison to the first's setup distance ( $2.9m$ ).

# Chapter 5

## Conclusions And Future Work

### 5.1 Conclusions

This work aimed in the development of PF algorithms for RF localization in real world environments. Bistatic scatter radio architecture was introduced in order to make the problem crystal clear and all the modules of the setup were thoroughly presented.

Apart from that RSSI and PF theory used in this work was included. In the end the simulation results proved that it all worked and especially the experimental results showing that this work can be applied in real world scenarios.

### 5.2 Future Work

This work only scratches the surface of RF localization on bistatic scatter radio networks. Estimating the path loss exponents is an unfinished problem that was not solved due to shortage of time and solving it is definitely a must for the future. Directionality of the reader's antenna can be exploited to enhance the results of this work. Apart from that, estimation of the Gamma parameters ( $m_1, m_2$ ) of the links is another goal for the future.

# Chapter 6

## Appendix

### 6.1 Proof for Product of Two Gamma Distributions

Here are the two PDFs:

$$f_{x_1}(x_1) = \frac{x_1^{m_{1,j}-1} e^{-\frac{x_1}{\theta_1}}}{\theta_1^{m_{1,j}} \Gamma(m_{1,j})},$$

$$f_{x_2}(x_2) = \frac{x_2^{m_2-1} e^{-\frac{x_2}{\theta_2}}}{\theta_2^{m_2} \Gamma(m_2)}.$$

Where,

$$\mathbb{E}[x_1] = m_{1,j}\theta_1 \rightarrow \theta_1 = \frac{\mathbb{E}[x_1]}{m_{1,j}}, \text{ and}$$
$$\mathbb{E}[x_2] = m_2\theta_2 \rightarrow \theta_2 = \frac{\mathbb{E}[x_2]}{m_2}.$$

In this case,

$$\mathbb{E}[x_1] = \mathbb{E}[x_2] = 1$$
$$\text{so } \rightarrow \theta_1 = \frac{1}{m_{1,j}} \text{ and } \theta_2 = \frac{1}{m_2}$$

$$f_x(x) = \int_{-\infty}^{+\infty} \frac{1}{x_1} f_{x_1}(x_1) f_{x_2}\left(\frac{x}{x_1}\right) dx_1, \quad (6.1)$$

but in this case  $x_1 \geq 0$ ,

so eq(6.1) becomes:

$$\begin{aligned} f_x(x) &= \\ &= \int_0^{+\infty} \frac{1}{x_1} f_{x_1}(x_1) f_{x_2}\left(\frac{x}{x_1}\right) dx_1 = \\ &= \frac{m_{1,j}^{m_{1,j}} m_2^{m_2} x^{m_2-1}}{\Gamma(m_{1,j}) \Gamma(m_2)} \int_0^{+\infty} x_1^{m_{1,j}-m_2-1} e^{-x_1 m_{1,j} \frac{x m_2}{x_1}} dx_1 \end{aligned} \quad (6.2)$$

and

$$\int_0^{+\infty} x^{v-1} e^{-\frac{\beta}{x} - \gamma x} dx = 2 \left(\frac{\beta}{\gamma}\right)^{\frac{v}{2}} K_v\left(2\sqrt{\beta\gamma}\right),$$

where  $K_v(\cdot)$  is the modified Bessel function of the second kind (eq. 3.471.9) [11]

so eq(6.2):

$$\begin{aligned} f_x(x) &= \\ &= \frac{m_{1,j}^{m_{1,j}} m_2^{m_2} x^{m_2-1}}{\Gamma(m_{1,j}) \Gamma(m_2)} 2 \left(\frac{m_2 x}{m_{1,j}}\right)^{\frac{m_{1,j}-m_2}{2}} K_{m_{1,j}-m_2}\left(2\sqrt{m_{1,j} m_2 x}\right), \end{aligned} \quad (6.3)$$

but since this is a linear function of the kind:  $y = ax$ ,  $x > 0$ ,  $a > 0$

$$f_y(y) = \frac{1}{|a|} f_x\left(\frac{y}{a}\right) \quad (6.4)$$

so (6.3) from (6.4) takes form:

$$\begin{aligned}
f_y(y) &= \\
&= 2 \left( \frac{m_{1,j} m_2 y}{a} \right)^{\frac{m_{1,j} + m_2}{2}} \frac{1}{\Gamma(m_{1,j}) \Gamma(m_2) y} K_{m_{1,j} - m_2} \left( 2 \sqrt{\frac{m_{1,j} m_2 y}{a}} \right). \quad (6.5)
\end{aligned}$$

But since this function is used for every particle distinctly:

$a_j^{[m]} = P_{TX} L_0(\mathbf{x}_T^{[m]}) L_j(\mathbf{x}_T^{[m]})$ , where  $^{[m]}$  is the particle index.

$$\begin{aligned}
f_{y|\mathbf{x}_t^{[m]}}(y; a_j^{[m]}, m_{1,j}, m_2) &= \\
&= 2 \left( \frac{m_{1,j} m_2 y}{a_j^{[m]}} \right)^{\frac{m_{1,j} + m_2}{2}} \frac{1}{\Gamma(m_{1,j}) \Gamma(m_2) y} K_{m_{1,j} - m_2} \left( 2 \sqrt{\frac{m_{1,j} m_2 y}{a_j^{[m]}}} \right) \quad (6.6)
\end{aligned}$$

# Bibliography

- [1] P. N. Alevizos, “Channel coding and detection for increased range bistatic scatter radio,” Master’s thesis, Technical University of Crete, Oct. 2014, supervisor A. Bletsas.
- [2] G. Vougioukas, “Extended range scatter radio links with embedded radio,” Undergraduate Thesis, Technical University of Crete, Jul. 2016, supervisor A. Bletsas.
- [3] S. D. Assimonis, S.-N. Daskalakis, and A. Bletsas, “Sensitive and Efficient RF Harvesting Supply for Batteryless Backscatter Sensor Networks,” *IEEE Trans. Microwave Theory Tech.*, vol. 64, no. 4, pp. 1327–1338, Apr. 2016.
- [4] S. N. Daskalakis, S. D. Assimonis, E. Kampianakis, and A. Bletsas, “Soil moisture wireless sensing with analog scatter radio, low power, ultra-low cost and extended communication ranges,” in *Proc. IEEE Sensors Conf. (Sensors)*, Valencia, Spain, Nov. 2014, pp. 122–125.
- [5] K. Tountas, “Implementation of frequency division multiple access digital backscatter sensor network,” Undergraduate Thesis, Technical University of Crete, Oct. 2014, supervisor A. Bletsas.
- [6] K. Tountas, P. N. Alevizos, A. Tzedaki, and A. Bletsas, “Bistatic architecture provides extended coverage and system reliability in scatter sensor networks,” in *Proc. International EURASIP Workshop on RFID Technology (EURFID)*, Rosenheim, Germany, Oct. 2015, pp. 144–151.
- [7] E. Alimpertis, “Smart sensors of rf and backscatter signals with localization,” Master’s thesis, Technical University of Crete, Aug. 2014, supervisor A. Bletsas.

- 
- [8] E. Alimpertis, N. Fasarakis-Hilliard, and A. Bletsas, “Community RF Sensing for Source Localization,” *IEEE Wireless Commun. Lett.*, vol. 3, no. 4, pp. 393–396, Aug. 2014.
- [9] S. Thrun, W. Burgard, and D. Fox, *Probabilistic Robotics*. Cambridge, MA: The MIT Press, 2006.
- [10] A. Pappoulis and S. U. Pillai, *Probability, Random Variables and Stochastic Processes*, 4th ed. New York, NY: McGraw-Hill, 2002.
- [11] I. S. Gradshteyn and I. M. Ryzhik, *Table of Integrals, Series, and Products*, 7th ed. Elsevier/Academic Press, Amsterdam, 2007.